



1 **Multifactor colorimetric analysis on pH-indicator papers: an**
2 **optimized approach for direct determination of ambient**
3 **aerosol pH**

4 Guo Li¹, Hang Su^{1*}, Nan Ma², Guangjie Zheng^{1†}, Uwe Kuhn¹, Meng Li¹, Thomas Klimach¹,
5 Ulrich Pöschl¹, Yafang Cheng^{1*}

6 ¹ Multiphase Chemistry Department, Max Planck Institute for Chemistry, Mainz, Germany

7 ² Institute for Environmental and Climate Research, Jinan University, Guangzhou, China

8 [†] Now at: Department of Energy, Environmental & Chemical Engineering, Center for Aerosol Science &
9 Engineering, Washington University, St. Louis, Missouri 63130, USA

10 * Correspondence to: Y. Cheng (yafang.cheng@mpic.de) or H. Su (h.su@mpic.de)

11

12 **Abstract**

13 Direct measurement of the acidity (pH) of ambient aerosol particles/droplets has long been a challenge for
14 atmospheric scientists. A novel and facile method was introduced recently by Craig et al. (2018), where the pH
15 of size-resolved aerosol droplets was directly measured by two types of pH-indicator papers (pH ranges: 0 – 2.5
16 and 2.5 – 4.5) combined with RGB-based colorimetric analyses using a model of G-B (G minus B) versus pH².
17 Given the wide pH range of ambient aerosols, we optimize the RGB-based colorimetric analysis on pH papers
18 with a wider detection range (pH ~ 0 to 6). Here, we propose a new model to establish the linear relationship
19 between RGB values and pH: $pH_{predict} = a \times R_{normal} + b \times G_{normal} + c \times B_{normal}$. This model shows a wider applicability
20 and higher accuracy than those in previous studies, and is thus recommended in future RGB-based colorimetric
21 analyses on pH papers. Moreover, we identify one type of pH paper (Hydrion® Brilliant pH dip sticks, Lot Nr.
22 3110, Sigma-Aldrich) that is more applicable for ambient aerosols in terms of its wide pH detection range (0 to 6)
23 and strong anti-interference capacity. The determined minimum sample mass (~ 180 µg) highlights its potential
24 to predict aerosol pH with a high time resolution (e.g., ≤ 1 hour). We further show that the routinely adopted way
25 of using pH color charts to predict aerosol pH may be biased by the mismatch between the standard colors on the
26 color charts and the real colors of investigated samples. Thus, instead of using the producer-provided color chart,
27 we suggest an in-situ calibration of pH papers with standard pH buffers.

28



29 **1 Introduction**

30 Aerosol particles have vital impacts on atmospheric chemistry, human health and global climate (Pöschl, 2005;
31 Baltensperger et al., 2008; Pósfai and Buseck, 2010; von Schneidemesser et al., 2015; Shiraiwa et al., 2017).
32 Understanding the basic physicochemical properties of aerosols can provide insights into various aerosol
33 processes in the atmosphere and may further help to establish measures against air pollution. Aerosol acidity,
34 usually quantified by aerosol pH, is one of the most important basic properties of liquid-phase aerosols. Aerosol
35 pH has multiple effects on the other properties of aerosols, e.g., aerosol composition (Cheng et al., 2016),
36 reactivity (Gao et al., 2004; Iinuma et al., 2004; Northcross and Jang, 2007), toxicity (Fang et al., 2017;
37 Chowdhury et al., 2018), phase transition (Dallemagne et al., 2016; Losey et al., 2018) and their related climatic
38 effects (Dinar et al., 2008; Hinrichs et al., 2016; Cai et al., 2018). It also plays a critical role during secondary
39 organic aerosol (SOA) formation (e.g., Surratt et al., 2007; Gaston et al., 2014; Han et al., 2016) and in many
40 other chemical processes in the atmosphere (Hennigan et al., 2015; Cheng et al., 2016; Wang et al., 2016; Keene
41 et al., 2004; Ahrens et al., 2012).

42
43 Despite its essential importance, currently there is few aerosol pH measurement data set available. One main
44 reason is the small sizes (with an aerodynamic diameter range of 2 nm – 10 µm, see McNeill, 2017) of these
45 atmospheric particles, rendering measurements of aerosol pH not as easy as for bulk solutions. Moreover, the
46 non-conservative nature of H⁺, i.e., H⁺ concentrations do not scale in proportion to the dilution levels due to
47 buffering effects and the partial dissociation of weak acids, further makes probe of aerosol pH a challenging topic
48 (Hennigan et al., 2015). For direct measurements of aerosol pH, two types of methods have been employed: filter-
49 based sample extraction (Koutrakis et al., 1988; Keene et al., 2002; Jang et al., 2008) and
50 spectroscopic/microscopic analysis (Li and Jang, 2012; Dallemagne et al., 2016; Rindelaub et al., 2016; Craig et
51 al., 2017; Wei et al., 2018). As the former method is offline, it suffers from both poor time resolution and intensive
52 labor work (Hennigan et al., 2015). Moreover, it cannot account for the water in the aerosol droplets, and involves
53 extraction with solvents that can shift the equilibria of present ions, leading to high uncertainties. The latter
54 method is normally used for laboratory-generated particles with simple compositions that cannot fully represent
55 ambient aerosols (Craig et al., 2018). Due to these limitations of direct measurements, thermodynamic
56 equilibrium models such as ISORROPIA-II (Fountoukis and Nenes, 2007) and E-AIM (Clegg and Seinfeld, 2006a,
57 b) have been widely used to estimate the acidity of ambient aerosol droplets, although comprehensive evaluations
58 of the acidity are hampered by lack of observational data. Thus, developing new methods to directly measure
59 ambient aerosol pH is imminently needed to constrain the output of thermodynamic models.

60
61 In a recent study, Craig et al. (2018) reported an intriguing way to directly measure aerosol pH using pH-indicator
62 papers, which in the past are the most common and convenient tool to test the pH of bulk solutions. To measure
63 aerosol pH, the generated size-resolved aqueous aerosol samples ((NH₄)₂SO₄-H₂SO₄) were firstly collected on
64 pH-indicator papers. Then the color of the samples on pH papers was analyzed quantitatively through a
65 colorimetric image processing program (Matlab). In this way, the standard pH color chart of the indicator papers
66 was used as a reference to finally derive the aerosol pH. The use of pH-indicator papers and the related color
67 processing technique introduced by Craig et al. (2018) tactfully circumvents the challenges and difficulties in
68 aerosol pH measurements. However, Craig et al. (2018) only reported two types of pH papers with relatively high



69 precision for pH measurements (one with pH range 0 - 2.5 and the other 2.5 – 4.5, see Craig et al., 2018), whereas
70 in the atmosphere the aerosol pH may vary in a wide range. Note that the authors indeed employed another type
71 of pH paper with a larger pH range from 0 to 6 for ambient aerosol sampling, unfortunately they found that this
72 paper was not compatible with their Matlab script for more quantitative analysis (Craig et al., 2018).

73
74 The colorimetric method used by Craig et al. (2018) was based on analyzing the red (R), green (G) and blue (B)
75 channels of the sample images, where a linear dependence of the difference between G and B (G-B) on pH^2 was
76 found. According to trichromatic theory, RGB are the three primary colors and their combination in varying
77 proportions can generate any other specific color (Su et al., 2008). The standard RGB scale is represented by the
78 values of R, G and B, and each has a range from 0 to 255. For example, the number [0, 0, 0], i.e., $R = 0$, $G = 0$,
79 $B = 0$, corresponds to absolute black and [255, 255, 255] to true white. RGB-based image analysis has been
80 applied in the fields of inorganic and analytical chemistry. For instance, Selva Kumar et al. (2018) found a good
81 linearity between concentrations of Thorium ions (Th^{4+}) and the ratio of R and G (R/G), and Wan et al. (2017)
82 reported a relation between bovine serum albumin (BSA) concentrations and the normalized values of R, G and
83 B, respectively. In these previous studies, different RGB models (i.e., ways to interpret the RGB values) were
84 adopted, however with few detailed explanations on the intrinsic reasons. To further enhance the reliability and
85 comparability of the data associated with RGB analysis, a unified model/method to deal with the RGB information
86 is needed, especially for the pH determination of aerosols where high uncertainty of measured pH values can have
87 a huge impact on the pH-dependent multiphase chemical processes.

88
89 Considering that the pH values of ambient aerosols can cover a wide range (up to ~ 6) (von Glasow and Sander,
90 2001; Pszenny et al., 2004; Song et al., 2018; Shi et al., 2019), the goal of the present study is to optimize the
91 RGB-based colorimetric analysis on pH-indicator papers for direct determination of ambient aerosol pH in a wider
92 detection range (pH ~ 0 to 6). We thus propose a new way to analyze the RGB values and establish the relationship
93 between RGB and pH. We further compare our proposed RGB model with the models used in previous studies
94 in terms of evaluating the established linear relationship between RGB and pH. Nine types of pH papers are tested
95 for their potential of probing pH of ambient aerosols. In addition, the routine way of using a pH color chart to
96 derive the pH of samples is inspected, and the results reveal some deficiencies of this method. Therefore, we
97 suggest an optimized way to use pH papers for aerosol pH prediction with higher precision and accuracy.

98 **2 Materials and Methods**

99 **2.1 pH-indicator papers**

100 Nine types of pH-indicator papers were adopted in this study. Each type has a pH color chart that is accompanied
101 with the pH papers and supposed to serve as a reference to quantify the pH of a sample through colorimetric
102 analysis. Details about the pH paper detection ranges and the corresponded type classification used in this work
103 can be found in Table S1. The first two types are the same as used by Craig et al. (2018), aiming to compare our
104 results with those from Craig et al. and validate our colorimetric image processing method. The others have larger
105 pH detection ranges covering the generally observed pH range of ambient aerosols. Note that in this study, we
106 mainly focused on the first five types of pH papers and the remaining four types were also evaluated and compared



107 with the first five types in terms of their resistance to chemical interference and potential capability to measure
108 the pH of ambient aerosols.

109 2.2 pH buffers and aerosol sample solutions

110 To examine the correlation between RGB and pH, eight standard pH buffer solutions were used as purchased and
111 meanwhile several other buffers (with different pH values as the purchased ones) were obtained by mixing the
112 commercial buffers with solutions of sodium hydroxide or hydrochloric acid (prepared using de-ionized water,
113 18.2 MΩ cm). pH values of all the buffers were further checked by a pH bench meter (model: HI 2020-02, Hanna
114 Instruments Inc., USA). Prior to the check, the pH meter was calibrated with a three-point calibration mode using
115 the standard buffer solutions provided by Hanna Instruments Inc., USA. The measured pH values and their
116 standard derivations are listed in Table S2, and the measured pH values show a small deviation from those
117 specified on the buffer solution bottles, within the displayed uncertainties concomitant with these specified values.
118 Considering that some inorganic/organic components of ambient aerosols might interfere with the dyes on pH
119 papers and cause biased estimation of pH, salt systems with varying inorganic and/or organic acids common in
120 aerosols and pH levels (as measured by the pH bench meter) were employed to test the applicability of different
121 types of pH papers combined with our RGB model. Details about the composition of the tested salt systems can
122 be found in Table S3. In general, the inorganic systems were similar to those used by Craig et al. (2018). Here,
123 we further tested the influence of organic acids on pH paper performance by adding organic acids into the
124 inorganic systems. As oxalic acid (C₂H₂O₄) and malonic acid (C₃H₄O₄) were frequently detected in tropospheric
125 aerosols and found to be the dominant short dicarboxylic acids in aerosol composition (Abbatt et al., 2005;
126 Falkovich et al., 2005), they were adopted in this study. For the solution preparation of each system, varying
127 amounts of 1 M inorganic/organic acids were added into 30 mM inorganic salt solution to achieve different pH
128 levels (Surratt et al., 2008; Craig et al., 2018). To prepare the inorganic and organic mixtures, the amount of
129 added organic acids was generally two times larger than the inorganic acids and the final salt concentration could
130 be as low as 15 mM due to the dilution effect of added acids. To prepare the solutions, all chemicals were used
131 as purchased: NaOH (≥ 99.0%, Roth, Germany), Na₂SO₄ (≥ 99.0%, Merck, Germany), NaNO₃ (≥ 99.0%, Merck,
132 Germany), Na₂CO₃ (≥ 99.5%, Sigma-Aldrich, USA), (NH₄)₂SO₄ (≥ 99%, Sigma-Aldrich, USA), NH₄NO₃ (≥
133 98.0%, Fisher Chemical, USA), MgSO₄ (> 98%, neoFroxx GmbH, Germany), H₂SO₄ (98%, Merck, Germany),
134 HNO₃ (65%, Merck, Germany), HCl (37%, Merck, Germany), C₂H₂O₄·2H₂O (≥ 99%, Sigma-Aldrich, USA) and
135 C₃H₄O₄ (99%, Sigma-Aldrich, USA).

136 2.3 Correlation between RGB and pH

137 Figure 1 shows the procedure of how to use a colorimetric analysis to obtain the correlation between RGB and
138 pH. First, 2 μL of liquid samples was dripped onto each piece of pH paper held by a clean transparent glass plate
139 (with the other side coated by a piece of graph paper). This adopted small volume (2 μL) was based on calculation
140 of the available amounts of liquid aerosols for aerosol sampling under a typically polluted conditions (with PM_{2.5}
141 mass concentration around 100 μg m⁻³) with high relative humidity (≥ 80%), and assuming a sampling flow rate
142 of several hundred liter per minute (e.g., can be achieved by a Tisch Environmental PM_{2.5} high volume air sampler,
143 see <https://tisch-env.com/high-volume-air-sampler/pm2.5>) and a sampling time of a few (2 - 4) hours. Note that,
144 to further reduce the sampling flow rate and time, we identified the minimum sample volume and mass needed to



145 generate a measurable color change on the suggested pH paper. The related results are shown below. Then an
146 image of the sample was captured by a smartphone camera (Apple iPhone 5s in this study) immediately. Similar
147 to Craig et al. (2018), the corresponding color chart of the used pH paper was included into each image to correct
148 for potential influences of variations of light source and angle during photographing. The digital images were
149 processed by an Adobe Photoshop software to crop a square with 100×100 pixels at the center of the sample (as
150 well as each color chip on the color chart). The RGB information of the cropped square was then obtained and
151 further analyzed by Matlab (The MathWorks, Inc. version R2018b).

152 2.4 RGB model

153 Considering that a color is represented by combination of R, G and B values, a linear combination of these three
154 primary colors should be able to reflect the characteristics of the color and therefore represent the pH related to
155 the color. Su et al. (2008) reported a good correlation between the linearly combined RGB and the contents of
156 chlorophyll *a* and lipid, respectively in microalgae. To further account for the effect of changing light intensity
157 on the obtained RGB values, each color channel should be normalized at first (Yadav et al., 2010). The
158 normalization can be achieved through Eqns. (1) – (3) shown below:

159

$$160 R_{\text{normal}} = R / (R + G + B) \quad (1)$$

$$161 G_{\text{normal}} = G / (R + G + B) \quad (2)$$

$$162 B_{\text{normal}} = B / (R + G + B) \quad (3)$$

163

164 where *R*, *G* and *B* are the mean value of each primary color on the entire 100×100 pixels image, respectively.
165 Note that every pixel has an RGB value vector: [R, G, B]. Then a model describing the linear combination of
166 RGB can be given as follows:

167

$$168 pH_{\text{predict}} = aR_{\text{normal}} + bG_{\text{normal}} + cB_{\text{normal}} \quad (4)$$

169

170 where the linear combination $aR_{\text{normal}} + bG_{\text{normal}} + cB_{\text{normal}}$ essentially represents the color information and here
171 can be treated as equivalent to the predicted pH (pH_{predict}) based on RGB analysis; *a*, *b* and *c* are the coefficients,
172 which can be determined by linear regression analysis through Matlab. The linear regression function is expressed
173 as:

$$174 Y = aX_1 + bX_2 + cX_3 \quad (5)$$

175

176 where *Y* is the dependent variable vector, *X*₁, *X*₂ and *X*₃ are independent variable vectors. These vectors can be
177 achieved from a standard color chart or a series of buffer samples (with known pH values) on pH papers: *Y* is the
178 series of pH values (i.e., reference pH, $pH_{\text{reference}}$) shown on the color chart or of buffer samples (as shown in Fig.
179 1, the pH papers with different pH buffer solutions are collected together to form a pH series); *X*₁, *X*₂ and *X*₃
180 are the normalized average of R, G and B respectively, based on analysis on the detected colors. As a color chart is
181 normally used as a reference for pH measurements using pH papers, a linear regression analysis on the color chart
182 can provide the coefficient vector [*a*, *b*, *c*] as an answer. Then the same set of coefficient vector (i.e., [*a*, *b*, *c*]) are



183 used to predict the pH (i.e., pH_{predict}) of aerosol samples using Eqn (4). Thus, with this RGB model, a linear
184 relationship between RGB-predicted pH (pH_{predict}) and reference pH ($pH_{\text{reference}}$) is expected for the calibration (as
185 shown in Fig. 1), in order to finally predict sample aerosol pH on a pH paper.

186 3 Results

187 3.1 Validation of the new RGB model

188 As the RGB model (i.e., G-B vs pH^2) used by Craig et al. (2018) produced good linear correlations for the two
189 types of pH papers that the authors adopted, we first examined the validity of this RGB model against the first
190 five types of pH papers used in this work. Note that here the first two types of pH papers are the ones used and
191 recommended by Craig et al. (2018). Figure S1 shows the relationship between average G-B and pH^2 derived
192 from the color charts of these five types of pH papers, respectively. Relatively good linear correlations can be
193 found for the first three types, which is consistent with Craig et al. (2018). However, non-monotonic correlations
194 are encountered for the last two types of pH papers, which are the ones with wider pH detection ranges (0.5 – 5.5
195 and 0 – 6, respectively). These results indicate a limited feasibility of the RGB model proposed by Craig et al.
196 (2018).

197
198 Thus, the validity of our new RGB model was further checked through the five types of pH papers. The colors
199 on the color chart for each type of pH paper were firstly analyzed through our RGB model and then the calculated
200 pH_{predict} were compared with the reference pH shown on the color chart. As shown in Fig. 2a-e (the ‘color chart’
201 column on the left-hand side), good linearity between pH_{predict} and $pH_{\text{reference}}$ can be observed for all these pH paper
202 types.

203
204 As aforementioned, besides the RGB model used by Craig et al. (2018), other models have also been adopted to
205 create a linear correlation between RGB and concentrations of the chemicals of interest in previous colorimetric
206 analyses (Su et al., 2008; Yadav et al., 2010; Wan et al., 2017; Selva Kumar et al., 2018). However, few
207 comparisons have been made regarding the goodness of the established linearity using these RGB models. Here
208 we further compared our model with the other two models (i.e., R/G vs pH and G-B vs pH^2) proposed by Selva
209 Kumar et al. (2018) and Craig et al. (2018) respectively, in terms of evaluating their correlation coefficient, R^2 .
210 Figure S2 (the ‘color chart’ panel on the left-hand side) displays the R^2 of the established linear correlation between
211 pH_{predict} and $pH_{\text{reference}}$ when the three models are used for the five types of pH papers, respectively. For the color-
212 chart-derived linear correlation, the model G-B vs pH^2 presents poor goodness-of-fit for type IV and V pH papers
213 (consistent with the results shown in Fig. S1). The model R/G vs pH shows relatively high R^2 for all the pH paper
214 types. Nevertheless, this RGB model still underperforms our model. Overall, our RGB model could provide a
215 high R^2 (> 0.95) for all the five types of pH papers, which demonstrates the universal validity of our RGB model.

216 3.2 Calibration with standard buffer solutions

217 A good linearity, however, may not always be obtained from the color chart of some types of pH papers in some
218 pH ranges. For example, in the ‘color chart’ column of Fig. 2, the pH_{predict} present small but discernable deviations
219 from $pH_{\text{reference}}$ for types I, III and IV pH papers. And the type V pH paper shows even larger differences at both



220 ends of the pH range. Similar phenomenon was also observed in the study of Craig et al. (2018) with their RGB
221 model, where they argued that the pH paper dye became less effective at the limits of the pH paper range, due to
222 the pK_a values of the dye were normally at the middle of the pH range. But it may also originate from some color
223 bias due to the differences between the experiment conditions and the ones under which the color chart is made
224 by the producer.

225
226 Thus, following the same procedure as for the color chart (see Fig. 1), pH papers with samples of a series of 2 μ L
227 standard buffer droplets were also measured. The pH values of the standard buffers were known beforehand and
228 further checked with a pH meter (also denoted as ' $pH_{reference}$ ', see Table S2). Figures 2f-j (the '2 μ L buffer' column
229 on the right-hand side) show the comparison between $pH_{predict}$ and $pH_{reference}$ for the samples of 2 μ L buffers. Much
230 better linearity between $pH_{predict}$ and $pH_{reference}$ can be observed for all the five types of pH papers. Especially, the
231 significant deviation of $pH_{predict}$ from $pH_{reference}$ found in the left panel (the 'color chart' column) disappear for the
232 type I and V pH papers. This means that the deviations at the edge of the pH range in the color-chart-derived
233 calibration curves are mainly due to the color bias of the color chart itself or caused during photographing.

234
235 Actually, even small deviations found in the color-chart-derived calibration curves (the 'color chart' column in
236 Fig. 2) may lead to significant or non-negligible errors in measuring aerosol pH. We conducted a case study using
237 the type IV pH paper combined with our RGB model to predict the pH of buffer samples by using the color-chart-
238 derived coefficient vector $[a, b, c]$, i.e., the color-chart-calibration method (Fig. 2d). The blue symbols in Fig. S3
239 represent $pH_{predict}$ versus $pH_{reference}$ of the standard buffer samples. Systematical underestimation of $pH_{predict}$ can
240 be found at the lower $pH_{reference}$ values (i.e., $pH_{reference} = 1, 1.68$ and 2) but a slight overestimation is observed at
241 $pH_{reference} = 5$. This significant discrepancy may be attributed to the mismatch between the reference colors on the
242 color chart and the real colors of the samples, due to the differences between our experiment conditions and the
243 ones under which the color chart is made by the producer. This gives us a hint that the coefficient vector derived
244 from the color chart is not suitable for predicting the pH of aerosol samples.

245
246 For the established linear relationship using 2 μ L standard buffers, the performances of different RGB models
247 were further compared and the results are shown in Fig. S2 (the '2 μ L buffer' panel on the right-hand side). Our
248 RGB model still outperforms the other two models for all the five types of pH papers employed in this work.
249 Overall, the good agreement between $pH_{predict}$ and $pH_{reference}$ for all these tested pH papers verifies the wide
250 applicability of our RGB model to the pH paper calibration using standard buffers. In the following section, we
251 will examine the quality of predicting samples pH with the standard-buffer-calibration method.

252 3.3 pH estimation for aerosol surrogates ((NH₄)₂SO₄-H₂SO₄) with the type IV and V pH papers

253 In order to test the feasibility of pH papers with larger pH detection ranges for pH prediction of aerosols, we
254 further used the type IV and V pH papers to estimate the pH of lab-prepared aerosol surrogates ((NH₄)₂SO₄ -
255 H₂SO₄). To minimize the effect of varying photographing conditions (e.g., angle, light variation) on the colors of
256 the captured image, experiments were carried out in a cupboard with a constant light source. In addition, the pH
257 paper samples as well as the smartphone were fixed on a small glass plate and a metal holder respectively, to keep
258 their position unchanged throughout the experiment. Note that applying the standard-buffer-derived coefficients



259 (Fig. 2i and 2j) for pH prediction of samples required the same constant light source conditions for sample imaging
260 processes as for standard buffers.

261

262 pH_{predict} versus $pH_{\text{reference}}$ for the samples on the type IV pH paper are shown in Fig. S4. Generally, the pH_{predict} by
263 the type IV pH paper are comparable with the $pH_{\text{reference}}$ at a lower pH range (i.e. $pH_{\text{reference}} = 0.46, 1.52$ and 3.0).
264 However, an obvious outlier with 1.5 unit of overestimation in pH_{predict} can be found at $pH_{\text{reference}}$ around 4 (outlier
265 highlighted by the arrow in Fig. S4). This overestimation was proved to be reproducible by our six replicate
266 experiments and it was even found for samples of diluted H_2SO_4 solutions with reference pH around 4 on the type
267 IV pH paper. Such overestimation may be due to the chemical interferences caused by the samples or the low
268 buffering levels of the samples. Thus, the type IV pH paper is not recommended for future pH measurements of
269 aerosols. However, it may still work well for the other sample types, such as found for our self-prepared phosphate
270 buffers (Fig. S4). On the other hand, the type V pH paper shows decent agreements between pH_{predict} and $pH_{\text{reference}}$
271 within the examined pH range, as shown in Fig. 3a. Moreover, the pH_{predict} are also compared with the results by
272 Craig et al. (2018). The orange and blue bars in Fig. 3a represent the measured pH ranges for the lab-generated
273 $(\text{NH}_4)_2\text{SO}_4 - \text{H}_2\text{SO}_4$ aerosols with particle sizes larger than $2.5 \mu\text{m}$ using pH papers (the same as the type I and II
274 pH papers used here) and Raman spectroscopy, respectively.

275 4 Discussion

276 4.1 Chemical interference

277 As aforementioned, aerosol samples with different compositions may have interferences on the indicating color
278 of a pH paper and thereby cause its poor performance for aerosol pH prediction, e.g., the overestimation of pH of
279 aerosol surrogates $(\text{NH}_4)_2\text{SO}_4\text{-H}_2\text{SO}_4$ with the Type IV pH paper. To test the capability of chemical resistance
280 of the Type V pH paper, we further tested its performance of predicting the pH of lab-prepared aerosol surrogates
281 with varying inorganic/organic compositions commonly exist in ambient aerosols.

282

283 Figure 4 displays pH_{predict} versus $pH_{\text{reference}}$ for our lab-prepared samples under different pH levels using the Type
284 V pH paper. As shown in Fig. 4a, systematic divergences between pH_{predict} and $pH_{\text{reference}}$ (i.e., overestimation of
285 pH_{predict} when $pH_{\text{reference}}$ is in the range of $2.5 - 3.5$ whereas underestimation of pH_{predict} when $pH_{\text{reference}} > \sim 4.5$)
286 can be found for these tested inorganic systems. Interestingly these mismatches disappear when the organic acids
287 are introduced into these inorganic systems (Fig. 4b), and also for the cases when the inorganic acids are replaced
288 by organic acids (Fig. S5). In Fig.4b, this good agreement for pH_{predict} versus $pH_{\text{reference}}$ is observed not only for
289 systems containing oxalic acid ($\text{C}_2\text{H}_2\text{O}_4$, solid markers) but also for those having malonic acid ($\text{C}_3\text{H}_4\text{O}_4$, hollow
290 markers) with an average deviation (of pH_{predict} from $pH_{\text{reference}}$) < 0.5 unit. The fact that the existence of organic
291 acids significantly improves the quality of pH_{predict} may be attributed to the enhanced buffering levels of the
292 samples (Fillion et al., 1999; Li et al., 2016). Actually, good agreement between pH_{predict} and $pH_{\text{reference}}$ is found
293 for both the inorganic and organic phosphate systems (Fig. S6) based on our further tests, which is probably due
294 to the high buffering levels of these systems maintained by the phosphate itself (Hourant, 2004). Nevertheless,
295 the solvent effect of the added organics on acid dissociation equilibria may also play a role (Padró et al., 2012).
296 The detailed mechanisms may need to be explored in future studies. Given the large contribution of organics



297 (Jimenez et al., 2009) and the well-known dominance of both organic acids (i.e., oxalic acid and malonic acid) in
298 ambient aerosols (Abbatt et al., 2005; Falkovich et al., 2005), the potential interferences found for the inorganic
299 systems can be expected to become vanished when organics are concomitant under ambient conditions.
300 Additionally, the interference check was also performed for the other pH paper types (type III and VI-IX) that
301 have larger pH detection ranges. Similar to the type IV pH paper, significant deviations of pH_{predict} from $pH_{\text{reference}}$
302 (≥ 1.5 unit) were observed for these types (see SI text and Fig. S7).

303 4.2 Identification of the needed minimum sample amount for the type V pH paper

304 The pH of ambient aerosols can be changing due to the varying atmospheric composition (e.g., some important
305 trace gases like SO_2 , NO_2 , NH_3 and organic acids) and physical characteristics (e.g., ambient relative humidity
306 and temperature). Thus, reflecting the temporal evolution of aerosol pH requires a pH measurement method with
307 a high time resolution. As aforementioned, to collect 2 μL of liquid aerosol samples, a sampling time of 2 – 4
308 hours is needed even using a high-volume air sampler with a sampling flow rate of several hundred liter per minute.
309 Here, in order to have a higher time resolution and/or a lower sampling flow rate, we further identified the
310 minimum sample volume needed to generate a measurable color change on the type V pH paper. Figure 3b shows
311 the results for 0.1 μL of lab-prepared aerosol samples. Similar to the RGB analysis procedure used for the 2 μL
312 samples (e.g., in Fig. 3a), the pH_{predict} in Fig. 3b are calculated with the averaged coefficient vector $[a, b, c]$ derived
313 from three replicate calibration experiments with 0.1 μL standard buffers (Fig. S8). Generally, pH_{predict} agrees
314 well with $pH_{\text{reference}}$, with biases (averaged pH_{predict} versus $pH_{\text{reference}}$) within 0.5 unit. Note that to avoid fast water
315 exchange between the lab air and our samples (aerosols/buffers) as well as potential interfering effects
316 (absorption/reaction) caused by the lab air, the 0.1 μL samples were transferred (through a pipette) directly onto
317 the pH paper surface and each sample was immediately photographed ($\leq \sim 3$ seconds) after it got contact with the
318 pH paper dye. Due to this extremely small sample volume, the influence of lab air on sample pH could become
319 prominent because a significant sample color change was frequently observed after the sample was exposed to
320 the lab air for $> \sim 5$ seconds.

321

322 These results confirm the feasibility of the type V pH paper as well as our RGB model for pH estimation of the
323 liquid aerosol samples with a volume even down to 0.1 μL . This tiny volume corresponds to a sample mass of ~
324 180 μg assuming an effective density of 1.8 g cm^{-3} for ambient aerosols (Sarangi et al., 2016; Geller et al., 2006),
325 which is comparably low to the needed minimum particulate masses in Craig et al. (2018), i.e., ~ 65 μg to ~ 2.5
326 mg for $\text{PM}_{2.5}$ or larger particles with pH from 0 – 2.5 to 2.5 - 4. According to our calculation, under typically
327 polluted conditions (with $\text{PM}_{2.5}$ mass concentration around 100 $\mu\text{g m}^{-3}$) with high relative humidity ($\geq 80\%$) to
328 collect aerosol samples with this even smaller mass/volume can be achieved by an air sampler with a sampling
329 flow rate of ~ 22 liter per minute and with a sampling time of ~ 1 hour. Alternatively, the sample time can be
330 further reduced to less than 1 hour (e.g., 0.5 hour) by adopting an air sampler with a relatively higher sampling
331 flow rate (e.g., ~ 45 liter per minute). The needed low sampling mass and the large pH detection range of the type
332 V pH paper highlight its potential for future development of real-time aerosol pH measurements. Moreover,
333 instead of using a color chart to calibrate pH papers for each sample (Craig et al., 2018), our results demonstrate
334 that the in-situ calibration method of using standard buffers (independent of different samples) can derive an
335 averaged coefficient vector $[a, b, c]$ which can be uniformly applied to pH prediction of different samples provided



336 the photographing conditions are kept constant. This unique feature further facilitates the application of the type
337 V pH paper under ambient cases.

338 **5 Conclusions**

339 We proposed a new model to establish the correlation between the color of samples on pH-indicator papers and
340 their measured pH. The model was based on RGB analysis of the images of samples. Comparison of our model
341 and another two RGB models verified the high reliability of our model. Using our RGB model, good agreement
342 between the model-predicted pH (pH_{predict}) and reference pH ($pH_{\text{reference}}$) for pH paper color charts as well as
343 standard buffers were observed for all the tested types of pH papers. Different types of pH papers with larger pH
344 detection ranges were further examined for their performance to predict the pH of lab-prepared aerosol samples
345 with varying inorganic/organic compositions common in ambient aerosols. The results suggest that only the type
346 V pH paper (with a pH range of ~ 0 - 6) deserves practical applications for pH measurements of ambient aerosols.
347 The minimum liquid sample mass/volume needed for the type V pH paper is identified as ~ 180 $\mu\text{g}/0.1 \mu\text{L}$, which
348 means that this type of pH paper can be applied to collect ambient aerosols with a high time resolution (e.g., ≤ 1
349 hour). Whereas the other types may suffer from some chemical interferences during pH measurements and
350 therefore can generate large biases for the measured pH of aerosols. The routine procedure of using pH papers to
351 estimate a sample pH was also examined in a case study using the type IV pH paper. The results show that
352 referring to the color chart for pH estimation (i.e. the color-chart-calibration method) may cause a bias of the
353 predicted pH. To use the pH papers in a more proper way, here we further demonstrated that the in-situ calibration
354 method of using standard buffers (independent of different samples) could derive an averaged coefficient vector
355 $[a, b, c]$, which can be uniformly applied to pH prediction of different samples provided the photographing
356 conditions are kept constant.

357 **Data availability**

358 The underlying research data and Matlab code can be accessed upon contact with Guo Li (guo.li@mpic.de),
359 Yafang Cheng (yafang.cheng@mpic.de) or Hang Su (h.su@mpic.de).

360 **Supplement**

361 The supplement is available in a separate file.

362 **Author contributions**

363 Y.C. and H.S. conceived and led the study. G.L. performed experiments and data analysis. Y.C., H.S., U.P., U.K.,
364 N.M., G.Z., M.L., T.K. discussed the results. G.L. and Y.C. wrote the manuscript with inputs from all co-authors.

365 **Competing interests**

366 The authors declare that they have no conflict of interest.



367 **Acknowledgement**

368 We acknowledge the National Natural Science Foundation of China (grant no. 91644218) and the National Key
369 Research and Development Program of China (grant no. 2017YFC0210104). This study was supported by the
370 Max Planck Society (MPG). G. L. acknowledges the financial support from the China Scholarship Council (CSC).
371 G. L. also would like to thank Ping Zhang, Jinqian Zhai and Yunkun Lang for their very helpful discussions
372 concerning the GRB model development.

373 **References**

- 374 Abbatt, J. P. D., Broekhuizen, K., and Pradeep Kumar, P.: Cloud condensation nucleus activity of internally
375 mixed ammonium sulfate/organic acid aerosol particles, *Atmospheric Environment*, 39, 4767-4778,
376 <https://doi.org/10.1016/j.atmosenv.2005.04.029>, 2005.
- 377 Ahrens, L., Harner, T., Shoeib, M., Lane, D. A., and Murphy, J. G.: Improved Characterization of Gas-Particle
378 Partitioning for Per- and Polyfluoroalkyl Substances in the Atmosphere Using Annular Diffusion Denuder
379 Samplers, *Environmental Science & Technology*, 46, 7199-7206, 10.1021/es300898s, 2012.
- 380 Baltensperger, U., Dommen, J., Alfarra, M. R., Duplissy, J., Gaeggeler, K., Metzger, A., Facchini, M. C.,
381 Decesari, S., Finessi, E., Reinnig, C., Schott, M., Warnke, J., Hoffmann, T., Klatzer, B., Puxbaum, H., Geiser,
382 M., Savi, M., Lang, D., Kalberer, M., and Geiser, T.: Combined Determination of the Chemical Composition
383 and of Health Effects of Secondary Organic Aerosols: The POLYSOA Project, *Journal of Aerosol Medicine and
384 Pulmonary Drug Delivery*, 21, 145-154, 10.1089/jamp.2007.0655, 2008.
- 385 Cai, J., Zhi, G., Yu, Z., Nie, P., Gligorovski, S., Zhang, Y., Zhu, L., Guo, X., Li, P., He, T., He, Y., Sun, J., and
386 Zhang, Y.: Spectral changes induced by pH variation of aqueous extracts derived from biomass burning
387 aerosols: Under dark and in presence of simulated sunlight irradiation, *Atmospheric Environment*, 185, 1-6,
388 <https://doi.org/10.1016/j.atmosenv.2018.04.037>, 2018.
- 389 Cheng, Y., Zheng, G., Wei, C., Mu, Q., Zheng, B., Wang, Z., Gao, M., Zhang, Q., He, K., Carmichael, G.,
390 Pöschl, U., and Su, H.: Reactive nitrogen chemistry in aerosol water as a source of sulfate during haze events in
391 China, *Science Advances*, 2, e1601530, 10.1126/sciadv.1601530, 2016.
- 392 Chowdhury, P. H., He, Q., Lasitza Male, T., Brune, W. H., Rudich, Y., and Pardo, M.: Exposure of Lung
393 Epithelial Cells to Photochemically Aged Secondary Organic Aerosol Shows Increased Toxic Effects,
394 *Environmental Science & Technology Letters*, 5, 424-430, 10.1021/acs.estlett.8b00256, 2018.
- 395 Clegg, S. L., and Seinfeld, J. H.: Thermodynamic Models of Aqueous Solutions Containing Inorganic
396 Electrolytes and Dicarboxylic Acids at 298.15 K. 1. The Acids as Nondissociating Components, *The Journal of
397 Physical Chemistry A*, 110, 5692-5717, 10.1021/jp056149k, 2006a.
- 398 Clegg, S. L., and Seinfeld, J. H.: Thermodynamic Models of Aqueous Solutions Containing Inorganic
399 Electrolytes and Dicarboxylic Acids at 298.15 K. 2. Systems Including Dissociation Equilibria, *The Journal of
400 Physical Chemistry A*, 110, 5718-5734, 10.1021/jp056150j, 2006b.
- 401 Craig, R. L., Nandy, L., Axson, J. L., Dutcher, C. S., and Ault, A. P.: Spectroscopic Determination of Aerosol
402 pH from Acid-Base Equilibria in Inorganic, Organic, and Mixed Systems, *The Journal of Physical Chemistry
403 A*, 121, 5690-5699, 10.1021/acs.jpca.7b05261, 2017.
- 404 Craig, R. L., Peterson, P. K., Nandy, L., Lei, Z., Hossain, M. A., Camarena, S., Dodson, R. A., Cook, R. D.,
405 Dutcher, C. S., and Ault, A. P.: Direct Determination of Aerosol pH: Size-Resolved Measurements of
406 Submicrometer and Supermicrometer Aqueous Particles, *Analytical Chemistry*, 90, 11232-11239,
407 10.1021/acs.analchem.8b00586, 2018.



- 408 Dallemagne, M. A., Huang, X. Y., and Eddingsaas, N. C.: Variation in pH of Model Secondary Organic Aerosol
409 during Liquid–Liquid Phase Separation, *The Journal of Physical Chemistry A*, 120, 2868-2876,
410 10.1021/acs.jpca.6b00275, 2016.
- 411 Dinar, E., Anttila, T., and Rudich, Y.: CCN Activity and Hygroscopic Growth of Organic Aerosols Following
412 Reactive Uptake of Ammonia, *Environmental Science & Technology*, 42, 793-799, 10.1021/es071874p, 2008.
- 413 Falkovich, A. H., Graber, E. R., Schkolnik, G., Rudich, Y., Maenhaut, W., and Artaxo, P.: Low molecular
414 weight organic acids in aerosol particles from Rondônia, Brazil, during the biomass-burning, transition
415 and wet periods, *Atmos. Chem. Phys.*, 5, 781-797, 10.5194/acp-5-781-2005, 2005.
- 416 Fang, T., Guo, H., Zeng, L., Verma, V., Nenes, A., and Weber, R. J.: Highly Acidic Ambient Particles, Soluble
417 Metals, and Oxidative Potential: A Link between Sulfate and Aerosol Toxicity, *Environmental Science &
418 Technology*, 51, 2611-2620, 10.1021/acs.est.6b06151, 2017.
- 419 Fillion, N., Probst, A., and Probst, J.-L.: Dissolved organic matter contribution to rain water, throughfall and soil
420 solution chemistry, *Analisis*, 27, 409-413, 1999.
- 421 Fountoukis, C., and Nenes, A.: ISORROPIA II: a computationally efficient thermodynamic equilibrium model
422 for
423 K^{+} – Ca^{2+} – Mg^{2+} – NH_4^{+}
424 $>$ – Na^{+} – SO_4^{2-} – NO_3^{-}
425 $^{-}$ – Cl^{-} – H_2O aerosols, *Atmos. Chem. Phys.*, 7,
426 4639-4659, 10.5194/acp-7-4639-2007, 2007.
- 427 Gao, S., Ng, N. L., Keywood, M., Varutbangkul, V., Bahreini, R., Nenes, A., He, J., Yoo, K. Y., Beauchamp, J.
428 L., Hodyss, R. P., Flagan, R. C., and Seinfeld, J. H.: Particle Phase Acidity and Oligomer Formation in
429 Secondary Organic Aerosol, *Environmental Science & Technology*, 38, 6582-6589, 10.1021/es049125k, 2004.
- 430 Gaston, C. J., Riedel, T. P., Zhang, Z., Gold, A., Surratt, J. D., and Thornton, J. A.: Reactive Uptake of an
431 Isoprene-Derived Epoxydiol to Submicron Aerosol Particles, *Environmental Science & Technology*, 48, 11178-
432 11186, 10.1021/es5034266, 2014.
- 433 Geller, M., Biswas, S., and Sioutas, C.: Determination of Particle Effective Density in Urban Environments with
434 a Differential Mobility Analyzer and Aerosol Particle Mass Analyzer, *Aerosol Science and Technology*, 40,
435 709-723, 10.1080/02786820600803925, 2006.
- 436 Han, Y., Stroud, C. A., Liggió, J., and Li, S. M.: The effect of particle acidity on secondary organic aerosol
437 formation from α -pinene photooxidation under atmospherically relevant conditions, *Atmos. Chem. Phys.*, 16,
438 13929-13944, 10.5194/acp-16-13929-2016, 2016.
- 439 Hennigan, C. J., Izumi, J., Sullivan, A. P., Weber, R. J., and Nenes, A.: A critical evaluation of proxy methods
440 used to estimate the acidity of atmospheric particles, *Atmos. Chem. Phys.*, 15, 2775-2790, 10.5194/acp-15-
441 2775-2015, 2015.
- 442 Hinrichs, R. Z., Buczek, P., and Trivedi, J. J.: Solar Absorption by Aerosol-Bound Nitrophenols Compared to
443 Aqueous and Gaseous Nitrophenols, *Environmental Science & Technology*, 50, 5661-5667,
444 10.1021/acs.est.6b00302, 2016.
- 445 Hourant, P.: General Properties of the Alkaline Phosphates: - Major Food and Technical Applications,
446 *Phosphorus Research Bulletin*, 15, 85-94, 10.3363/prb1992.15.0_85, 2004.
- 447 Iinuma, Y., Böge, O., Gnauk, T., and Herrmann, H.: Aerosol-chamber study of the α -pinene/O₃ reaction:
448 influence of particle acidity on aerosol yields and products, *Atmospheric Environment*, 38, 761-773,
449 <https://doi.org/10.1016/j.atmosenv.2003.10.015>, 2004.
- 450 Jang, M., Cao, G., and Paul, J.: Colorimetric Particle Acidity Analysis of Secondary Organic Aerosol Coating
451 on Submicron Acidic Aerosols, *Aerosol Science and Technology*, 42, 409-420, 10.1080/02786820802154861,
452 2008.



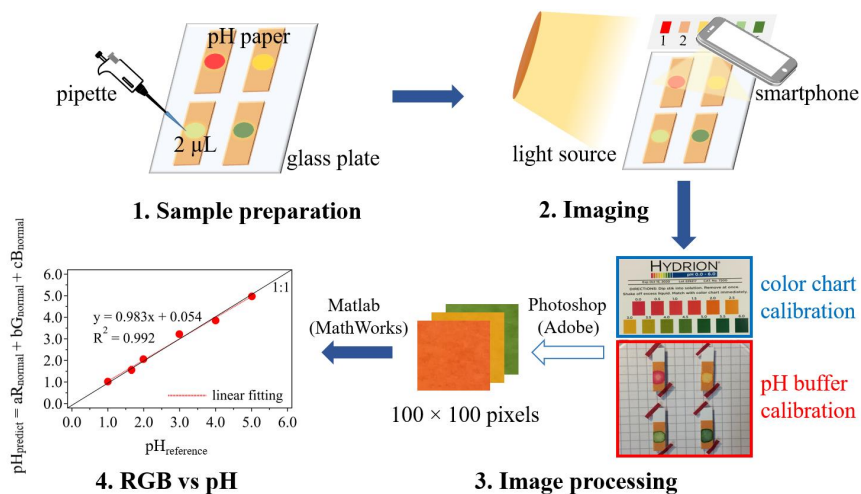
- 453 Jimenez, J. L., Canagaratna, M. R., Donahue, N. M., Prevot, A. S. H., Zhang, Q., Kroll, J. H., DeCarlo, P. F.,
454 Allan, J. D., Coe, H., Ng, N. L., Aiken, A. C., Docherty, K. S., Ulbrich, I. M., Grieshop, A. P., Robinson, A. L.,
455 Duplissy, J., Smith, J. D., Wilson, K. R., Lanz, V. A., Hueglin, C., Sun, Y. L., Tian, J., Laaksonen, A.,
456 Raatikainen, T., Rautiainen, J., Vaattovaara, P., Ehn, M., Kulmala, M., Tomlinson, J. M., Collins, D. R.,
457 Cubison, M. J., Dunlea, J., Huffman, J. A., Onasch, T. B., Alfarra, M. R., Williams, P. I., Bower, K., Kondo, Y.,
458 Schneider, J., Drewnick, F., Borrmann, S., Weimer, S., Demerjian, K., Salcedo, D., Cottrell, L., Griffin, R.,
459 Takami, A., Miyoshi, T., Hatakeyama, S., Shimojo, A., Sun, J. Y., Zhang, Y. M., Dzepina, K., Kimmel, J. R.,
460 Sueper, D., Jayne, J. T., Herndon, S. C., Trimborn, A. M., Williams, L. R., Wood, E. C., Middlebrook, A. M.,
461 Kolb, C. E., Baltensperger, U., and Worsnop, D. R.: Evolution of Organic Aerosols in the Atmosphere, *Science*,
462 326, 1525-1529, 10.1126/science.1180353, 2009.
- 463 Keene, W. C., Pszenny, A. A. P., Maben, J. R., and Sander, R.: Variation of marine aerosol acidity with particle
464 size, *Geophysical Research Letters*, 29, 5-1-5-4, 10.1029/2001gl013881, 2002.
- 465 Keene, W. C., Pszenny, A. A. P., Maben, J. R., Stevenson, E., and Wall, A.: Closure evaluation of size-resolved
466 aerosol pH in the New England coastal atmosphere during summer, *Journal of Geophysical Research:*
467 *Atmospheres*, 109, 10.1029/2004jd004801, 2004.
- 468 Koutrakis, P., Wolfson, J. M., and Spengler, J. D.: An improved method for measuring aerosol strong acidity:
469 Results from a nine-month study in St Louis, Missouri and Kingston, Tennessee, *Atmospheric Environment*
470 (1967), 22, 157-162, [https://doi.org/10.1016/0004-6981\(88\)90308-3](https://doi.org/10.1016/0004-6981(88)90308-3), 1988.
- 471 Li, H., Liu, F., Kang, L., and Zheng, M.: Study on the buffering capacity of wort, *Journal of the Institute of*
472 *Brewing*, 122, 138-142, 10.1002/jib.286, 2016.
- 473 Li, J., and Jang, M.: Aerosol Acidity Measurement Using Colorimetry Coupled With a Reflectance UV-Visible
474 Spectrometer, *Aerosol Science and Technology*, 46, 833-842, 10.1080/02786826.2012.669873, 2012.
- 475 Losey, D. J., Ott, E.-J. E., and Freedman, M. A.: Effects of High Acidity on Phase Transitions of an Organic
476 Aerosol, *The Journal of Physical Chemistry A*, 122, 3819-3828, 10.1021/acs.jpca.8b00399, 2018.
- 477 McNeill, V. F.: Atmospheric Aerosols: Clouds, Chemistry, and Climate, *Annual Review of Chemical and*
478 *Biomolecular Engineering*, 8, 427-444, 10.1146/annurev-chembioeng-060816-101538, 2017.
- 479 Northcross, A. L., and Jang, M.: Heterogeneous SOA yield from ozonolysis of monoterpenes in the presence of
480 inorganic acid, *Atmospheric Environment*, 41, 1483-1493, <https://doi.org/10.1016/j.atmosenv.2006.10.009>,
481 2007.
- 482 Padró, J. M., Acquaviva, A., Tascon, M., Gagliardi, L. G., and Castells, C. B.: Effect of temperature and solvent
483 composition on acid dissociation equilibria, I: Sequenced pKa determination of compounds commonly used as
484 buffers in high performance liquid chromatography coupled to mass spectroscopy detection, *Analytica Chimica*
485 *Acta*, 725, 87-94, <https://doi.org/10.1016/j.aca.2012.03.015>, 2012.
- 486 Pöschl, U.: Atmospheric Aerosols: Composition, Transformation, Climate and Health Effects, *Angewandte*
487 *Chemie International Edition*, 44, 7520-7540, 10.1002/anie.200501122, 2005.
- 488 Pósfai, M., and Buseck, P. R.: Nature and Climate Effects of Individual Tropospheric Aerosol Particles, *Annual*
489 *Review of Earth and Planetary Sciences*, 38, 17-43, 10.1146/annurev.earth.031208.100032, 2010.
- 490 Pszenny, A. A. P., Moldanová, J., Keene, W. C., Sander, R., Maben, J. R., Martinez, M., Crutzen, P. J., Perner,
491 D., and Prinn, R. G.: Halogen cycling and aerosol pH in the Hawaiian marine boundary layer, *Atmos. Chem.*
492 *Phys.*, 4, 147-168, 10.5194/acp-4-147-2004, 2004.
- 493 Rindelaub, J. D., Craig, R. L., Nandy, L., Bondy, A. L., Dutcher, C. S., Shepson, P. B., and Ault, A. P.: Direct
494 Measurement of pH in Individual Particles via Raman Microspectroscopy and Variation in Acidity with
495 Relative Humidity, *The Journal of Physical Chemistry A*, 120, 911-917, 10.1021/acs.jpca.5b12699, 2016.
- 496 Sarangi, B., Aggarwal, S. G., Sinha, D., and Gupta, P. K.: Aerosol effective density measurement using
497 scanning mobility particle sizer and quartz crystal microbalance with the estimation of involved uncertainty,
498 *Atmos. Meas. Tech.*, 9, 859-875, 10.5194/amt-9-859-2016, 2016.



- 499 Selva Kumar, R., Kumar, S. K. A., Vijayakrishna, K., Sivaramakrishna, A., Brahmananda Rao, C. V. S.,
500 Sivaraman, N., and Sahoo, S. K.: Development of the Smartphone-Assisted Colorimetric Detection of Thorium
501 by Using New Schiff's Base and Its Applications to Real Time Samples, *Inorganic Chemistry*, 57, 15270-
502 15279, 10.1021/acs.inorgchem.8b02564, 2018.
- 503 Shi, G., Xu, J., Shi, X., Liu, B., Bi, X., Xiao, Z., Chen, K., Wen, J., Dong, S., Tian, Y., Feng, Y., Yu, H., Song,
504 S., Zhao, Q., Gao, J., and Russell, A. G.: Aerosol pH dynamics during intense haze periods in an urban
505 environment in China: use of detailed, hourly, speciated observations to study the role of ammonia availability
506 and secondary aerosol formation and urban environment, *Journal of Geophysical Research: Atmospheres*, 0,
507 10.1029/2018jd029976, 2019.
- 508 Shiraiwa, M., Ueda, K., Pozzer, A., Lammel, G., Kampf, C. J., Fushimi, A., Enami, S., Arangio, A. M.,
509 Fröhlich-Nowoisky, J., Fujitani, Y., Furuyama, A., Lakey, P. S. J., Lelieveld, J., Lucas, K., Morino, Y., Pöschl,
510 U., Takahama, S., Takami, A., Tong, H., Weber, B., Yoshino, A., and Sato, K.: Aerosol Health Effects from
511 Molecular to Global Scales, *Environmental Science & Technology*, 51, 13545-13567, 10.1021/acs.est.7b04417,
512 2017.
- 513 Song, S., Gao, M., Xu, W., Shao, J., Shi, G., Wang, S., Wang, Y., Sun, Y., and McElroy, M. B.: Fine-particle
514 pH for Beijing winter haze as inferred from different thermodynamic equilibrium models, *Atmos. Chem. Phys.*,
515 18, 7423-7438, 10.5194/acp-18-7423-2018, 2018.
- 516 Su, C.-H., Fu, C.-C., Chang, Y.-C., Nair, G. R., Ye, J.-L., Chu, I.-M., and Wu, W.-T.: Simultaneous estimation
517 of chlorophyll a and lipid contents in microalgae by three-color analysis, *Biotechnology and Bioengineering*, 99,
518 1034-1039, 10.1002/bit.21623, 2008.
- 519 Surratt, J. D., Lewandowski, M., Offenberg, J. H., Jaoui, M., Kleindienst, T. E., Edney, E. O., and Seinfeld, J.
520 H.: Effect of Acidity on Secondary Organic Aerosol Formation from Isoprene, *Environmental Science &
521 Technology*, 41, 5363-5369, 10.1021/es0704176, 2007.
- 522 Surratt, J. D., Gómez-González, Y., Chan, A. W. H., Vermeylen, R., Shahgholi, M., Kleindienst, T. E., Edney,
523 E. O., Offenberg, J. H., Lewandowski, M., Jaoui, M., Maenhaut, W., Claeys, M., Flagan, R. C., and Seinfeld, J.
524 H.: Organosulfate Formation in Biogenic Secondary Organic Aerosol, *The Journal of Physical Chemistry A*,
525 112, 8345-8378, 10.1021/jp802310p, 2008.
- 526 von Glasow, R., and Sander, R.: Variation of sea salt aerosol pH with relative humidity, *Geophysical Research
527 Letters*, 28, 247-250, 10.1029/2000GL012387, 2001.
- 528 von Schneidemesser, E., Monks, P. S., Allan, J. D., Bruhwiler, L., Forster, P., Fowler, D., Lauer, A., Morgan,
529 W. T., Paasonen, P., Righi, M., Sindelarova, K., and Sutton, M. A.: Chemistry and the Linkages between Air
530 Quality and Climate Change, *Chemical Reviews*, 115, 3856-3897, 10.1021/acs.chemrev.5b00089, 2015.
- 531 Wan, Z., Zhong, L., Pan, Y., Li, H., Zou, Q., Su, K., and Wang, P.: Portable Microplate Analyzer with a
532 Thermostatic Chamber Based on a Smartphone for On-site Rapid Detection, *Analytical Sciences*, 33, 1291-
533 1296, 10.2116/analsci.33.1291, 2017.
- 534 Wang, G., Zhang, R., Gomez, M. E., Yang, L., Levy Zamora, M., Hu, M., Lin, Y., Peng, J., Guo, S., Meng, J.,
535 Li, J., Cheng, C., Hu, T., Ren, Y., Wang, Y., Gao, J., Cao, J., An, Z., Zhou, W., Li, G., Wang, J., Tian, P.,
536 Marrero-Ortiz, W., Secret, J., Du, Z., Zheng, J., Shang, D., Zeng, L., Shao, M., Wang, W., Huang, Y., Wang,
537 Y., Zhu, Y., Li, Y., Hu, J., Pan, B., Cai, L., Cheng, Y., Ji, Y., Zhang, F., Rosenfeld, D., Liss, P. S., Duce, R. A.,
538 Kolb, C. E., and Molina, M. J.: Persistent sulfate formation from London Fog to Chinese haze, *Proceedings of
539 the National Academy of Sciences*, 113, 13630-13635, 10.1073/pnas.1616540113, 2016.
- 540 Wei, H., Vejerano, E. P., Leng, W., Huang, Q., Willner, M. R., Marr, L. C., and Vikesland, P. J.: Aerosol
541 microdroplets exhibit a stable pH gradient, *Proceedings of the National Academy of Sciences*, 115, 7272-7277,
542 10.1073/pnas.1720488115, 2018.
- 543 Yadav, S. P., Ibaraki, Y., and Dutta Gupta, S.: Estimation of the chlorophyll content of micropropagated potato
544 plants using RGB based image analysis, *Plant Cell, Tissue and Organ Culture (PCTOC)*, 100, 183-188,
545 10.1007/s11240-009-9635-6, 2010.



546 **List of Figures:**



547

548

549 **Figure 1:** Schematic of using the RGB-based colorimetric method for pH estimation. For the color-chart-calibration method,
 550 both the color chart and the standard buffer samples are imaged into one digital photo for subsequent processing. For the
 551 standard-buffer-calibration method, only the standard buffer samples are used for imaging. Note that when using the standard-
 552 buffer-calibration results to predict the pH of aerosol samples, the photographing conditions for the samples are the same as
 553 those of the buffer calibration.

554

555

556

557

558

559

560

561

562

563

564

565

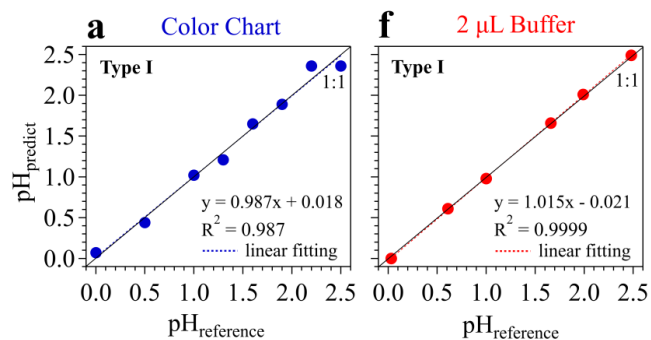
566

567

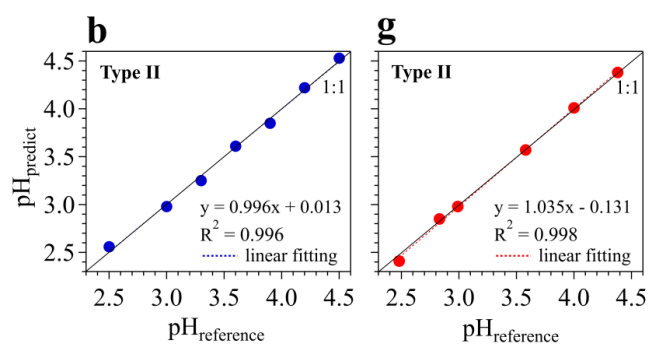
568

569

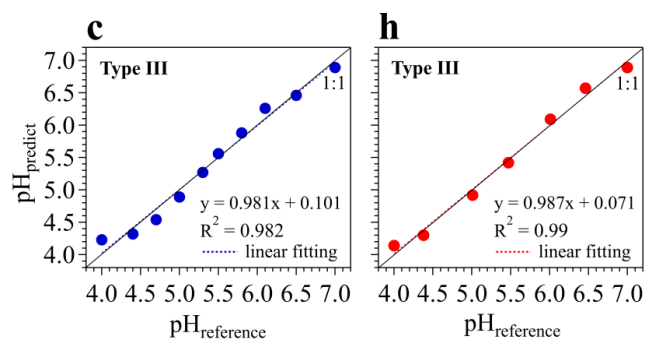
570



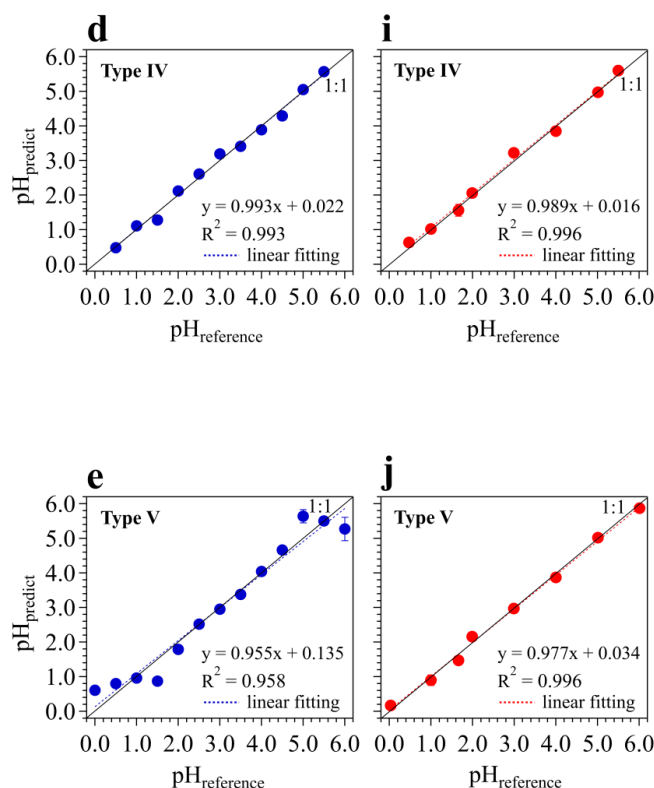
571



572



573



574

575

576

577 **Figure 2:** Predicted pH (pH_{predict}) using our RGB model versus the reference pH shown on the color chart and the pH-meter-
578 probed-pH of the buffer samples (all denoted as $pH_{\text{reference}}$) respectively, for the five different pH papers: (a) and (f) Type I: 0
579 – 2.5, (b) and (g) Type II: 2.5 – 4.5, (c) and (h) Type III: 4.0 – 7.0, (d) and (i) Type IV: 0.5 – 5.5 and (e) and (j) Type V: 0 –
580 6.0. Blue symbols denote the established relationship based on color charts only. Red symbols represent the results for 2 μL
581 of buffer droplets on pH papers. The error bars represent the standard deviation of five to six replicate experiments. Note that
582 the error bars in most of the panels are smaller than the symbols.

583

584

585

586

587

588

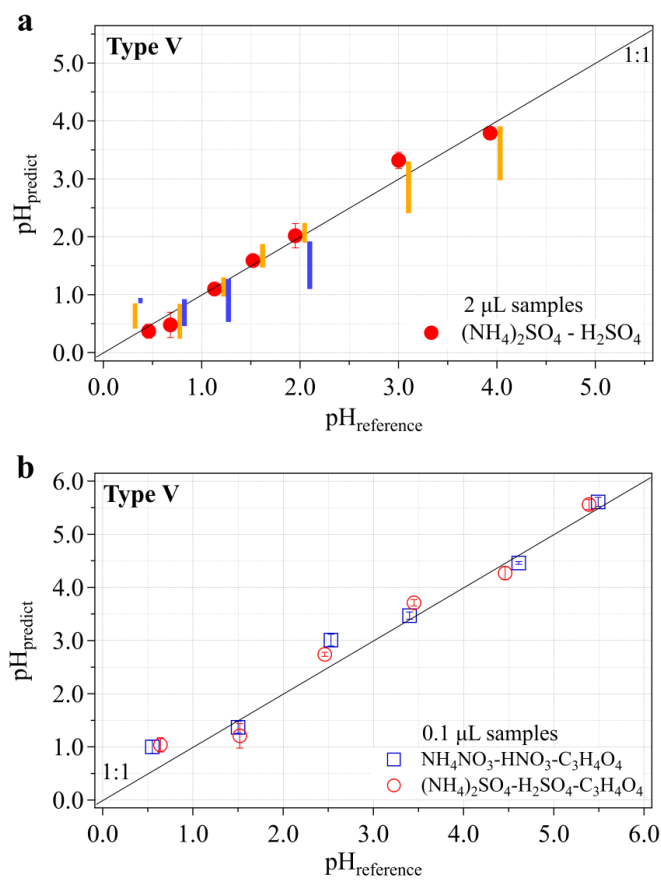
589

590

591

592

593



594

595

596

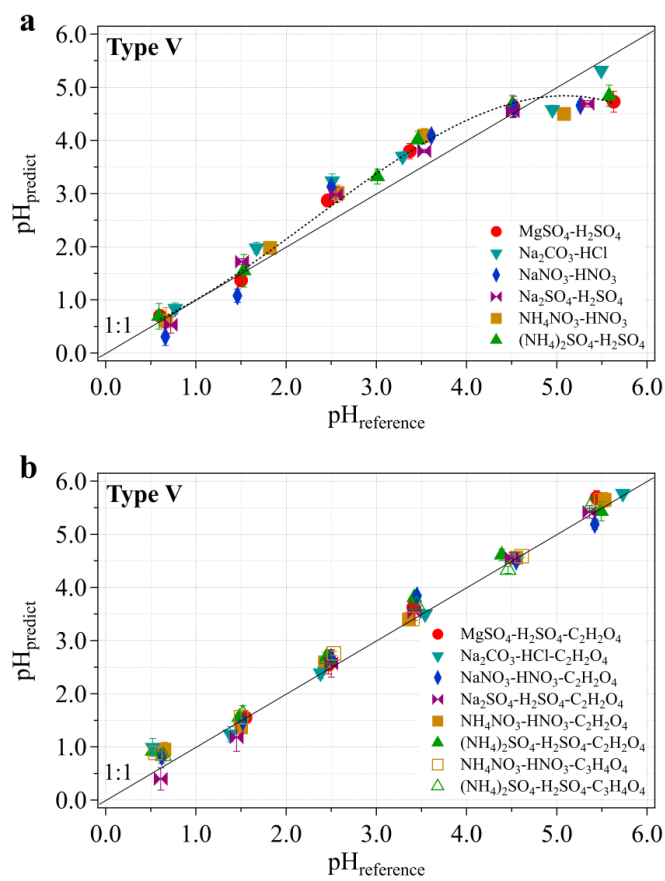
597 **Figure 3:** pH estimation using the type V pH paper for samples with different volumes: (a) 2 μL and (b) 0.1 μL . $\text{pH}_{\text{predict}}$ are
598 calculated with the averaged coefficient vector $[a, b, c]$ derived from three to six replicate experiments with the same amounts
599 of standard buffers as of the samples under constant photographing conditions. The error bars represent the standard deviation
600 of three to six replicate experiments. In (a), the heights of the orange and blue bars indicate the reported pH ranges measured
601 with pH papers and Raman spectroscopy respectively, for $(\text{NH}_4)_2\text{SO}_4 - \text{H}_2\text{SO}_4$ aerosols with particle sizes larger than 2.5 μm
602 in Craig et al. (2018). Each orange or blue bar has the same $\text{pH}_{\text{reference}}$ as of the red symbol close to it. In (b), for processing the
603 digital images of the 0.1 μL samples, a square with 20×20 pixels at the center of the samples is cropped for subsequent
604 colorimetric analyses.

605

606

607

608



609

610

611

612 **Figure 4:** pH estimation using the type V pH paper for salt systems with only inorganic acids (a) and both inorganic and
613 organic acids (b). $\text{pH}_{\text{predict}}$ are calculated with the averaged coefficient vector $[a, b, c]$ derived from three replicate calibration
614 experiments with standard buffers and under constant photographing conditions. The error bars represent the standard
615 deviation of three to four replicate experiments. The dotted line in (a) is used to guide the eye.

616